

Stabilizer Entropy and entanglement complexity in the Sachdev-Ye-Kitaev model

Barbara Jasser^{1,2,*}, Jovan Odavić^{2,3,†} and Alioscia Hamma^{1,2,3‡}

¹*Scuola Superiore Meridionale, Largo S. Marcellino 10, 80138 Napoli, Italy*

²*Istituto Nazionale di Fisica Nucleare (INFN), Sezione di Napoli, Italy and*

³*Dipartimento di Fisica ‘Ettore Pancini’, Università degli Studi di Napoli Federico II, Via Cintia 80126, Napoli, Italy*

The Sachdev-Ye-Kitaev (SYK) model is of paramount importance for the understanding of both strange metals and a microscopic theory of two-dimensional gravity. We study the interplay between Stabilizer Rényi Entropy (SRE) and entanglement entropy in both the ground state and highly excited states of the SYK4+SYK2 model interpolating the highly chaotic four-body interactions model with the integrable two-body interactions one. The interplay between these quantities is assessed also through universal statistics of the entanglement spectrum and its anti-flatness. We find that SYK4 is indeed characterized by a complex pattern of both entanglement and non-stabilizer resources while SYK2 is non-universal and not complex. We discuss the fragility and robustness of these features depending on the interpolation parameter.

Introduction.— The Sachdev-Ye-Kitaev (SYK) model [1, 2] describes the behavior of strongly correlated fermions in strange metals [3]. In recent years, the model has gained new interest from the high-energy community due to its holographic duality [4–6]. In the infra-red limit and large number of degrees of freedom, the model acquires conformal symmetry. The leading corrections to the out-of-time-ordered four-point correlation functions exhibit exponential growth over time. The rate of this growth reaches the universal upper bound established in [7], see [8, 9]. The low-energy sector of the SYK4 model is governed by an emergent reparametrization symmetry, described by Jackiw-Teitelboim (JT) gravity [6], providing insight into the holographic description of black holes and their thermodynamic properties. In quantum thermodynamics, the SYK model has been studied for its potential to show quantum advantage as a quantum battery [10–12], with a super extensive charging power [13].

The interpolation between the four-body (SYK4) and the two-body (SYK2) model [14, 15] provides a connection to a model of strongly correlated electrons. The two theories are very different: the SYK4 is chaotic, with an exponential density of states at low energy, while the SYK2 is integrable, with a polynomially vanishing gap. Remarkably, both models exhibit a volume law for entanglement [16]. One might wonder what makes these two regimes so different. Entanglement has been deeply investigated to better understand both the chaotic nature of SYK models [16–18] and their connection to holographic theory and complex quantum systems [3, 19, 20] but the transition to SYK2 shows that entanglement alone is not enough.

The second layer of quantum complexity is given by non-stabilizerness [21], a crucial resource in the context of universal quantum computation, error correction [22–26] and quantum simulation [27–30]. Recently, non-stabilizerness has risen to prominence due to finding a

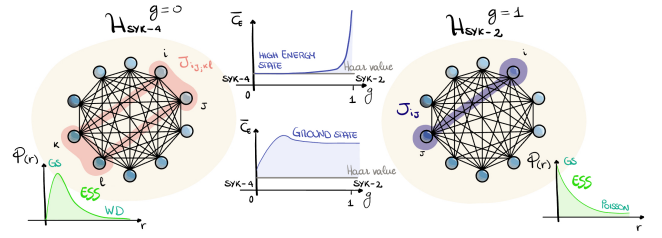


Figure 1: Schematic representation of the SYK₄+SYK₂ model $H(g)$ (see Eq. (5)). The left side ($g = 0$) corresponds to SYK₄ featuring the Wigner-Dyson entanglement spectrum statistics (ESS) in the ground state and near-universal capacity of entanglement C_E . On the right side ($g = 1$) the SYK₂ model is shown, exhibiting Poisson ESS and non-universal C_E . In the ground state, these features are fragile for SYK₄ and robust for SYK₂. Conversely, in high energy states the SYK₄ properties extend to every value of $g \neq 1$ making the SYK₂ features the fragile ones.

unique computable monotone for pure states, the Stabilizer Rényi Entropy (SRE) [31]. In the context of high-energy physics, both SRE and entanglement are studied for heavy nuclei simulations [32] and neutrino physics [33, 34]. Moreover, the delocalization due to the entanglement of non-stabilizerness resources has recently been connected to the holographic dual of back-reaction in the context of AdS-CFT [35], features of CFT [36, 37], and the harvesting of quantum resources from the vacuum of a quantum field [38, 39]. When entanglement delocalizes and scrambles non-stabilizer resources, this gives rise to universal behavior of out-of-time-order correlation functions, entanglement fluctuations [40, 41] and the onset of chaotic behavior in quantum many-body systems [42–44] in the ETH-MBL transition [45–48]. On the other hand, the fine structure of entanglement revealed by the statistics of entanglement gaps (ESS) [43, 49, 50] reaches the complex universal patterns of random matrix theory thanks to non-stabilizerness.

* b.jasser@ssmeridionale.it

† jovan.odavic@unina.it

‡ alioscia.hamma@unina.it

The main goal of this Letter is to study the SYK4+SYK2 model beyond perturbative limits under the lens of the emergence of quantum complex behavior from interplay between entanglement and SRE. We find that SYK4 exhibits a complex interplay of entanglement and SRE both in the ground state and in the high-energy eigenstates (middle of the spectrum), while SYK2 shows patterns of this interplay that are typical of integrable or non-chaotic models [51]. This is revealed by the adherence of SYK4 to Haar-like behavior for entanglement entropy, entanglement eigenvalues, and gaps statistics, capacity of entanglement, higher values of SRE, especially in its non-local features. On the other hand, SYK2 shows a lower level of SRE, and non-universal statistics in all the figures of merit mentioned above.

An important question is how robust are these behaviors in the SYK4+SYK2 model. The universal properties of SYK4 are fragile in the ground state: for every $g > 0$ the system falls into the SYK2 class. On the other hand, high-energy states show a reversed behavior. The SYK4 phase extends to every value of $g < 1$. These findings enrich those of [14] based on Green's functions. In addition, we also show that adherence of the energy spectrum to Wigner-Dyson universal behavior is fragile for SYK4+SYK2. Finally, we show that the behavior of SRE in the ground state is capable of classifying the 8-fold way of the symmetries of SYK4. A similar conclusion is also shown for the energy gap above the ground state. In order to argue about the robustness of these features, we apply quantum-information theoretic tools like the Kullback-Leibler divergence fidelity.

The model.— The most general form of SYK models [4, 52] considers a q -body all-to-all interaction between N Majorana fermionic modes. The Hamiltonian in terms of Majorana operators reads

$$H_q = (i)^{q/2} \sum_{1 \leq i_1 < \dots < i_q \leq N} J_{i_1 i_2 \dots i_q} \chi_{i_1} \chi_{i_2} \dots \chi_{i_q} \quad (1)$$

with q an even integer number. The disorder in the model is due to the couplings J_{i_1, i_2, \dots, i_q} which are identical, independent distributed (i.i.d.) gaussian variables with vanishing mean and variance

$$\overline{J_{i_1, i_2, \dots, i_q}} = 0; \quad \overline{J_{i_1, i_2, \dots, i_q}^2} = \frac{(q-1)! J}{N^{q-1}}. \quad (2)$$

For $q > 2$, the system exhibits quantum chaos [53, 54], as evidenced by several established indicators. One key probe is level repulsion in the energy spectra, characterized by the statistical distribution of energy level spacings [55–58]. This indicates that the eigenstates of the Hamiltonian are highly delocalized and correlated, a hallmark of quantum chaos. The system is defined on a complete graph, so the interactions are strongly non-local. Using the Jordan-Wigner transformations it is possible to map the Majorana operators into Pauli spin strings, used in the numerical simulations [59]. Notice that each spin operator can be expressed in terms of two Majorana

operators. Therefore, the total number of Majorana operators is double the number of Paulis. The simplest version of SYK models is the SYK2

$$H_2 = i \sum_{1 \leq i < j \leq N} J_{i,j} \chi_i \chi_j. \quad (3)$$

Since the interactions between fermions are considered in pairs, SYK2 represents the free fermions point of the theory. This results in Gaussian statistics for its spectral properties, meaning that it does not show the same level of randomness and complexity found in chaotic systems [5, 60]. The SYK2 model serves as a simple example of a disordered fermionic system and is analytically solvable [16]. The four-body interaction model, called SYK4, is

$$H_4 = - \sum_{1 \leq i < j < k < l \leq N} J_{i,j,k,l} \chi_i \chi_j \chi_k \chi_l. \quad (4)$$

This model satisfies the usual probes of quantum chaos [53, 54], i.e. the Hamiltonian exhibits level repulsion in its spectrum. The SYK4+SYK2 model is defined as [14]

$$H_g := (1-g)H_4 + gH_2, \quad (5)$$

with $g \in [0, 1]$. In the following, we compute by exact diagonalization the energy spectrum of H_g together with the exact ground state (GS) and middle-spectrum eigenstate (MS) for a number of realization M of the disorder. The eigenvalues of the reduced density operator (RDM) to half-system ρ_R will be denoted by $\{\lambda_k\}$ and are sorted in ascending order.

Entanglement.— To quantify the bipartite entanglement of the interpolated model, we focus on Rényi entropies defined as

$$S_\alpha = \frac{1}{1-\alpha} \log \text{Tr}[\rho_R^\alpha], \quad \alpha \in [0, 1) \cup (1, \infty), \quad (6)$$

The von Neumann entanglement entropy $S(\rho_R)_1 = -\text{Tr}(\rho_R \log(\rho_R))$ corresponds to the limit $\alpha \rightarrow 1^+$.

For random quadratic Hamiltonians, a class of models to which the SYK2 Hamiltonian belongs [16], the average ground-state entanglement entropy was derived in closed form in [61], given by

$$\mathcal{S}_1^{\text{SYK2}}(R, f) = \mathcal{K}(f) \ln(2)R, \quad (7)$$

where

$$\mathcal{K}(f) = \left[1 - \frac{1 + f^{-1}(1-f) \ln(1-f)}{\ln 2} \right]. \quad (8)$$

Here, $f = R/N^{\text{spin}}$ represents the ratio between the subsystem size R and the total system size in terms of the number of qubits. The entanglement entropy scaling of the SYK2 ground state follows a volume law (extensive scaling with subsystem size) but with a coefficient dependent on the ratio f , distinguishing it from the fully quantum chaotic regime in the thermodynamic limit.

Efforts to extend these insights to the SYK4 model include works such as Refs. [17, 62, 63]. On the other hand, the maximally chaotic random pure state, sampled uniformly according to the Haar measure, exhibits the Page value for entanglement entropy, given by

$$\frac{2S_1^{\text{Haar}}}{N \ln(2)} = 2f, \quad \text{for } f \in [0, 1/2], \quad (9)$$

to leading order in the system size [64, 65].

In Fig. 2, we present the results for the rescaled entanglement entropy in the GS and MS of H_g of the interpolated SYK Hamiltonian, with $f = 1/2$. The averaging is performed over different partitions of the system (denoted with an overline \bar{S}) [66] and multiple disorder realizations (denoted with $\langle \rangle_M$) of the model for each value of the interpolation parameter g . Details of the realization and disorder statistics for various system sizes are provided in [67]. We see that for $g = 0$ (SYK4) the GS is closer than $g = 1$ (SYK2) to the Haar value, although none of them reaches the universal value. On the contrary, for MS, the relative gap ΔS_1 shows a perfect adherence of SYK4 with Haar value unlike SYK2 as it is shown by the finite-size scaling in the inset. The behavior with g suggests that the MS universal properties are valid for all $g \neq 1$, making SYK4 robust from this point of view. A similar analysis has been conducted for SYK4 in [17].

A finer probe into the structure of entanglement is given by the full distribution of the eigenvalues of the RDM. The reference Haar value is related to the Marchenko-Pastur (M-P) distribution as the limiting distribution of eigenvalues of Wishart matrices and reads $\eta^{\text{Haar}}(x) = 1 - \frac{2}{\pi} (x\sqrt{1-x^2} + \arcsin x)$; see [42, 68]. To distinguish two probability distributions we employ the Kullback-Leibler divergence $D_{KL}(p||q) := \sum_i p_i (\log p_i - \log q_i)$. The results in the top row of Fig. 3 show the

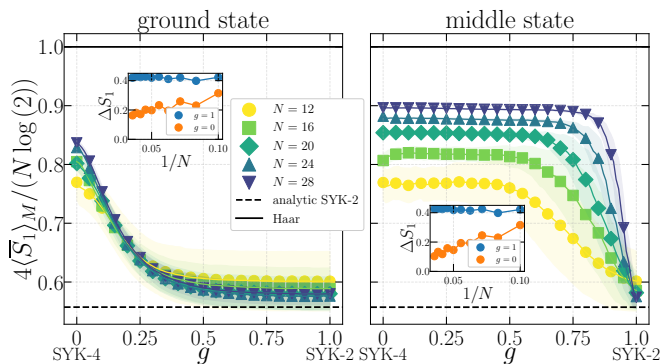


Figure 2: Averaged bipartite entanglement in the GS (left panel) and MS (right panel) of the SYK4+SYK2 model H_g as a function of g . Shaded areas represent the standard deviation across M realizations of the Hamiltonian. We define $\Delta S_1 := |(S_1 - S_1^{\text{Haar}})/S_1^{\text{Haar}}|$ the relative gap with the Haar (Page) value. The inset shows the finite size scaling of the relative gap ΔS_1 for $g = 0, 1$.

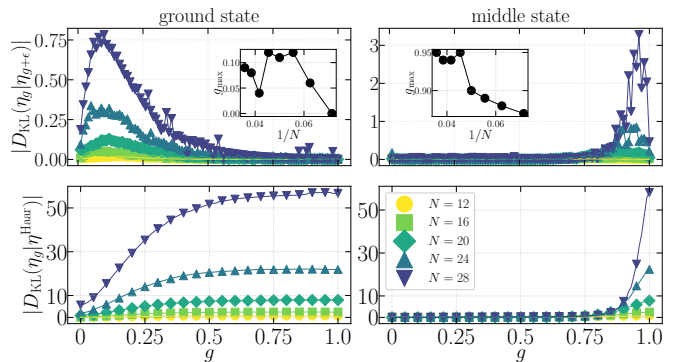


Figure 3: Renormalized RDM eigenvalues of half-subsystem. The reference value is the Marchenko-Pastur (M-P) distribution $\eta^{\text{Haar}}(x)$. We define $\eta_k = k/d$ and $x_k = (1/2)\sqrt{\lambda_k d}$ where $d = 2^{N/4}$ for $f = 1/2$.

fidelity $D_{KL}(\eta_g|\eta_{g+\epsilon})$ between two distributions of the eigenvalues of the RDM for two nearby values $g, g + \epsilon$ of the interpolation parameter. This quantity can serve as a probe of a sharp transition associated with an observable consisting of a probability distribution. We see that the GS and MS behave in symmetric and opposite ways. The structure of the eigenvalues of the RDM of the GS shows a sharp transition at $g > 0$ and then smooths out. On the other hand, for the MS, $g = 1$ is fragile and the eigenvalues of the RDM of highly excited states are smoothly varying all the way as long as SYK4 interactions are different from zero. The second row of Fig. 3 shows the same statistical distance between the state for the value g and the reference Haar value. While SYK4 is converging to the Haar value, SYK2 shoots away. The robustness of the two phases for GS and MS respectively is confirmed. In other words, for every value of $g \neq 1$, the eigenvalues of the RDM of highly excited states obey the universal Haar behavior.

Entanglement Spectrum Statistics (ESS).— Complex pattern of entanglement is characterized by universal properties of the statistics of the gaps in the entanglement spectrum, the so-called *entanglement spectrum statistics* (ESS) [49]. While chaotic systems, for instance, non-integrable systems obeying the eigenstate thermalization hypothesis (ETH) feature a universal, Wigner-Dyson (WD) behavior for the ESS, integrable, disordered free-fermion models feature a Poisson statistics in both the high energy states and the long time behavior away from equilibrium. Hybrid cases like MBL systems feature deviations from WD in polynomial time after a quantum quench [45]. The transition between the two regimes is due to the injection of non-stabilizer resources, which need to be scrambled around [43, 69].

From the perspective of random matrix theory, if the eigenvalues of the reduced density matrix are uncorrelated, the distribution is Poissonian. Conversely, correlated eigenvalues follow the Wigner-Dyson universality class. This observation underscores that the entanglement patterns between the two interpolating regimes

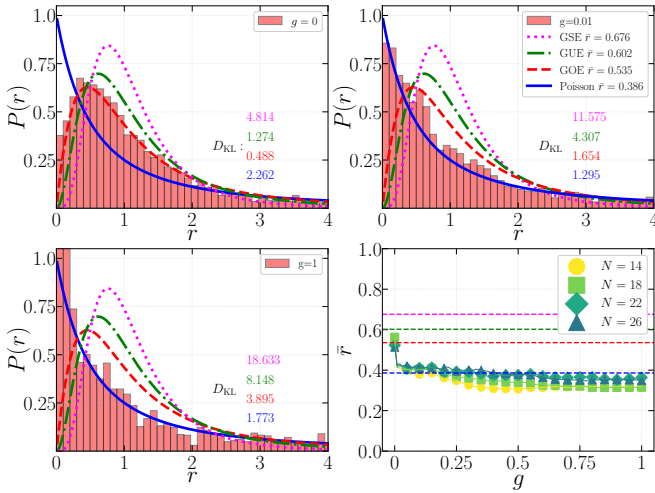


Figure 4: ESS of the GS RDM eigenvalues of the H_g model for different values of g . We superimpose the analytical curves for the Wigner-Dyson (dashed) and Poisson (blue continuous) distribution for comparison. System size $N = 22$ and number of realizations is $M = 100$. The number of bins used for the histogram is 100. The colored numbers represent the KL divergence of data against known distributions [67]

exhibit differing complexities. We focus on the probability density function (PDF) of the consecutive spacing ratios denoted as $P(r)$. To evaluate it we use the ascending eigenvalues $\{\lambda_k\}$ of the reduced density matrix and determine the spacing ratio as $r_k = \frac{\lambda_{k+1} - \lambda_k}{\lambda_k - \lambda_{k-1}}$, where $k = 2, 3, \dots, 2^R - 1$. The resulting ratios $\{r_k\}$ are plotted as a normalized histogram, excluding rare outliers with $r_j > 10.0$ to ensure proper normalization and accurate binning [70, 71]. The explicit functional forms of the corresponding Poisson and Wigner-Dyson Gaussian ensembles are provided in [72]. To complement this type of analysis, we also evaluate the averaged consecutive spacing ratio, defined as $\bar{r} = \langle \frac{\min(s_{k,j}, s_{k+1,j})}{\max(s_{k,j}, s_{k+1,j})} \rangle_{2^R-2, M}$ where the spacings are given by $s_{k,j} = \lambda_{k+1,j} - \lambda_{k,j}$, and the index $j = 1, 2, \dots, M$ refers to the different reduced density matrices considered across ensemble or disorder realizations.

In Fig. 4, we compute the ESS $P(r)$ for different realizations of the GS of the H_g model for several values of g . SYK4 ($g = 0$) adheres to the universal WD distribution for GOE as it is expected for a real Hamiltonian. As soon as the model is perturbed by SYK2, the distribution starts getting closer to Poisson. In the lower right panel of Fig. 4, we show the behavior of the averaged consecutive spacing ratio \bar{r} as a function of g , which shows a sudden jump as one moves from $g = 0$. We can see that this feature of the entanglement complexity which is typical of chaotic systems is fragile in the model. Similar results hold for the MS, see [67].

Stabilizer Rényi Entropy (SRE)— Non-stabilizerness is an essential property for universal quantum computa-

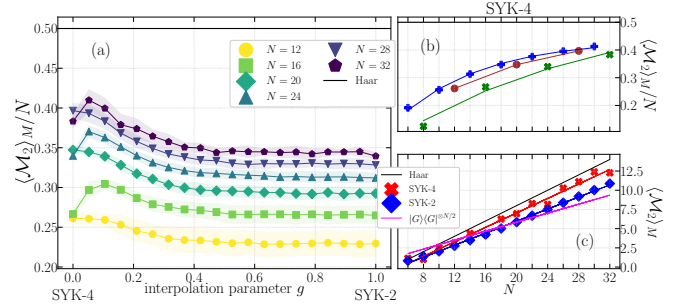


Figure 5: Ensemble averaged SRE \mathcal{M}_2 in the GS of the H_g . Panel (a): For all g the ground states exhibit a non-vanishing amount of non-stabilizerness. Panel (b): The non-monotonicity can be easily captured by a grouping of points: green crosses for $N \bmod 8 = 0$, blue for $N \bmod 8 = 2, 6$, and red circles for $N \bmod 8 = 4$. The lines represent fits [67]. Panel (c): SRE without the normalization with the system size as compared to the Haar value. $|G\rangle\langle G|$ is a single qubit state which maximizes SRE [67].

tion [73]. To quantify this property, we use the Stabilizer Rényi Entropy (SRE) [31], defined as

$$\mathcal{M}_\alpha(\Psi) = \frac{1}{1-\alpha} \log_2 \left(d^{-1} \sum_{P \in \mathcal{P}_N} |\text{Tr}(\Psi P)|^{2\alpha} \right). \quad (10)$$

Here, Ψ is the density matrix of a N -qubit state $|\Psi\rangle$, $d = 2^N$ is the Hilbert space dimension, and \mathcal{P}_N is the N -qubit Pauli group. The SREs for $\alpha \geq 2$ are good resource monotones [74]. Stabilizer entropies measure how far a state deviates from stabilizer states by analyzing its spread in the Pauli operator basis [31, 75]. The SRE stands out among non-stabilizerness monotones as it can be efficiently evaluated without the need for minimization procedures. In this work, we adopt the methodology outlined in Ref. [65] to compute the SRE. Specifically, we transform the ground state vectors obtained from exact diagonalization into matrix product state (MPS) tensor representations and employ the Perfect Sampling algorithm [76–78].

In Fig. 5, we show the numerical results for the scaling of SRE in the GS of the H_g model. From panel (a), we observe that the SYK-4 ($g = 0$) case exhibits a higher degree of non-stabilizer resources compared to the SYK-2 ($g = 1$) limit. From Fig. 5 (a), we observe that the SRE of the SYK-4 ground states does not exhibit a consistent monotonic increase with fermion number N , but instead shows a non-monotonic dependence. A more detailed analysis in Fig. 5 (b) reveals an oscillatory pattern in the SRE. The data is grouped and labeled according to the values of $N \bmod 8$, as indicated in the captions. Each of the three groups corresponds to a distinct exponent of the damped exponential. This grouping is motivated by the observation in [20], where it was first noted that the SYK-4 Hamiltonian exhibits

a particular particle-hole symmetry. The authors linked this symmetry to different Gaussian random matrix universality classes: GOE for $N \bmod 8 = 0$, GUE for $N \bmod 8 = 2, 6$, and GSE for $N \bmod 8 = 4$, which manifest in the Hamiltonian's spectrum. We observe the effects of this symmetry specifically in the ground state, without considering the full Hamiltonian spectrum. In contrast to entanglement (see Fig. 2) and ground state energy [79], the SRE appears to be much more sensitive to the finiteness of N . This highlights the unique ability of SRE to reveal hidden structures within many-body systems. A recent, striking example is the ability of SRE to detect a quantum phase transition that is not captured by entanglement in a system without a conventional order parameter [80].

How does the average SRE evolve as the system size increases for the ground state of the SYK-4 Hamiltonian? This behavior is depicted in panel (c) of Fig. 5. By fitting the data to a linear function [81], we obtain the following expression for the average SRE:

$$\langle \mathcal{M}_2 \rangle_M^{\text{fit}} \sim -2.4 + 0.95 \frac{N}{2}. \quad (11)$$

For Haar random states, it is known that

$$\mathcal{M}_2^{\text{Haar}} = -2 + \frac{N}{2}, \quad (12)$$

to leading order in the system size [31, 65, 82]. The factor 2 in the denominator of the linear term arises because $N/2$ represents the support of the spin/qubit representation. Our results show that the SYK-4 ground states slightly deviate from the characteristics of fully quantum chaotic and universal states, with a linear prefactor difference of approximately 0.05 when compared to Haar random states. A similar deviation was recently observed in the entanglement of middle-of-the-spectrum states in the SYK-4 model [17]. This provides evidence that low-temperature states, such as the ground states, fail to reach full universality.

Anti-Flatness.— A crucial point in the understanding of the relationship between SRE and entanglement comes from the realization that stabilizer states must have a flat entanglement spectrum [83]. Indeed, one can show that there is a strict relationship between the lack of flatness of the entanglement spectrum of the RDM and the SRE of the full state. In [84] it is shown that the linear SRE is exactly proportional to the average anti-flatness defined on a subsystem as $\mathcal{F} := \text{Tr}[\rho_R^3] - \text{Tr}^2[\rho_R^2]$. Another measure of anti-flatness is a numerically and analytically accessible quantity that is the logarithmic anti-flatness [65]

$$F(\rho_R) := 2(S_2(\rho_R) - S_3(\rho_R)). \quad (13)$$

In Supplementary Material [67], an excellent agreement across all system sizes is observed with the analytical results we derive for the SYK2 ($g = 1$) limit where we obtained a closed-form expression for the logarithmic anti-

flatness

$$F^{\text{SYK2}}(R, f) = 2R(1-f) \sum_{n=1}^{\infty} \frac{1}{n} \left(\frac{1}{2^n} - \frac{1}{2} \frac{3^n}{4^n} \right) \times {}_2F_1\left(\frac{1}{2}, 1-n, 2, 4f(1-f)\right) \quad (14)$$

where ${}_2F_1(a, b, c, d)$ is a hypergeometric function, $n > 0$, and $0 < f \leq 1/2$. For Haar random state in the large N limit the logarithmic anti-flatness approach system-size-independent value of $F^{\text{Haar}} = \log(5/4) \approx 0.223$ [65].

One of the most useful measures of anti-flatness comes from the modular entropy [85]

$$\tilde{S}_\alpha := \alpha^2 \partial_\alpha \left(\frac{\alpha - 1}{\alpha} S_\alpha \right). \quad (15)$$

Its derivative with respect to the Rényi parameter at $\alpha = 1$ is minus the variance of the entanglement Hamiltonian $H_\rho := -\log \rho$ defined as

$$-\text{Var}_\rho(H_\rho) := -\langle \log^2 \rho \rangle_\rho + \langle \log \rho \rangle_\rho^2 = \partial_\alpha \tilde{S}_\alpha \Big|_{\alpha=1} \quad (16)$$

It is also known as capacity of entanglement C_E and it is yet another measure of anti-flatness [86–88]. This quantity is relevant because it quantifies the amount of non-local SRE, that is, the SRE that cannot be undone by local unitary operations [35]. For Haar random states, one can compute [88, 89]

$$\partial_\alpha \tilde{S}_\alpha^{\text{Haar}} \Big|_{\alpha=1} = \frac{11}{4} - \frac{\pi^2}{3} \approx -0.539868. \quad (17)$$

which we use in our analysis as a reference value.

In Fig. 6, we compute the capacity of entanglement C_E as a probe of non-local SRE as a function of g in both the GS and MS of H_g . We see that SYK4 features a Haar-value capacity of entanglement, which is in perfect agreement in the MS. The finite-size scaling of the inset shows again the symmetric behavior of robustness observed earlier: while for the GS the SYK4 features are fragile, they are robust and can be extended all the way for any $g < 1$ for the MS.

Conclusions and Outlook.— In this paper, we studied the interplay between entanglement and non-stabilizer resources in the SYK4+SYK2 model through several figures of merit that involve probes into the non-local character of stabilizer entropy, the entanglement spectrum statistics, and the adherence of such quantities to predictions from random matrix theory. We show that SYK4 features a complex pattern of this interplay while the integrable SYK2 is not universal. Moreover, we show the robustness of the universal features of SYK4 and find that they vary greatly between the ground state and highly excited states. For this reason, it would be interesting to study the behavior of such interplay away from equilibrium and its role in operator scrambling [91]. The quantum advantage of SYK batteries could be related to an optimal usage of both entanglement [92] and non-stabilizer resources [93–95].

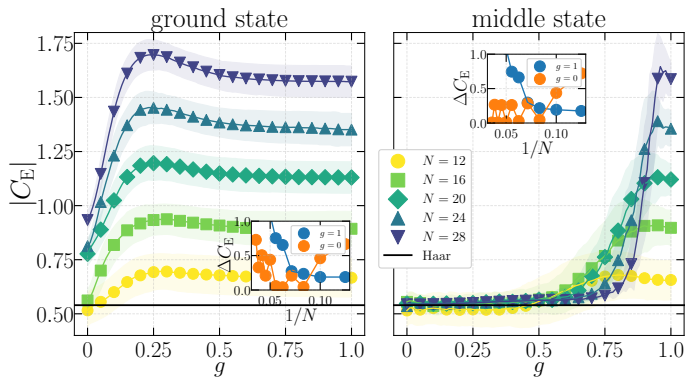


Figure 6: Ensemble averaged half-system capacity of entanglement in the GSs (left panel) and MSs (right panel) of H_g . The inset shows how the relative gap defined as $\Delta C_E = |(C_E - C_E^{\text{Haar}})/C_E^{\text{Haar}}|$ of $g=0$ (SYK4-) and $g=1$ (SYK2-) scales with respect to the Haar value. More on the C_E in the SYK-2 can be found in [90].

One of the most striking features of SYK4 is its dual

JT gravity at low temperature. We have shown that SYK4 is fragile under a two-body perturbation in the ground state while robust at high-energy, leaving open the question of its robustness at low temperature, which we plan to answer in a future work.

Acknowledgments.— Upon completion of this paper, we stumbled onto arXiv:2502.01582 which has a similar scope with our work. An early version of our work was presented at the poster session of the first workshop on many-body quantum magic (MBQM2024), TII Abu Dhabi in November 2024: *Barbara Jasser, Chaos, Entanglement and Stabilizer Entropy in SYK model*. AH and JO acknowledge support from the PNRR MUR project PE0000023-NQSTI. AH acknowledges support from the PNRR MUR project CN 00000013-ICSC. This work has been funded by project code PIR01 00011 ‘IBISCO’, PON 2014-2020, for all three entities (INFN, UNINA and CNR). Additionally, acknowledge ISCRa for awarding this project access to the LEONARDO super-computer, owned by the EuroHPC Joint Undertaking, hosted by CINECA (Italy) under the project ID: PQC - HP10CQQ3SR. We acknowledge stimulating conversations with P. Zanardi and Lorenzo Campos Venuti.

-
- [1] S. Sachdev and J. Ye, Physical Review Letters **70**, 3339–3342 (1993).
- [2] KITP, “Proceedings of the kitp,” (2015), <http://online.kitp.ucsb.edu/online/entangled15/kitaev/>, <http://online.kitp.ucsb.edu/online/entangled15/kitaev2/>.
- [3] D. Chowdhury, A. Georges, O. Parcollet, and S. Sachdev, Reviews of Modern Physics **94**, 035004 (2022).
- [4] A. Kitaev, Entanglement in strongly-correlated quantum matter, 38 (2015).
- [5] G. Sarosi, “Ads₂ holography and the syk model,” in *Proceedings of XIII Modave Summer School in Mathematical Physics — PoS(Modave2017)*, Vol. 323 (SISSA Medialab, 2018) p. 001.
- [6] D. A. Trunin, Physics-Uspexhi **64**, 219–252 (2021).
- [7] J. Maldacena, S. H. Shenker, and D. Stanford, Journal of High Energy Physics **2016**, 106 (2016).
- [8] N. Tsuji and P. Werner, Physical Review B **99**, 115132 (2019).
- [9] Y. Gu, A. Kitaev, and P. Zhang, Journal of High Energy Physics **2022**, 133 (2022).
- [10] F. Campaioli, S. Gherardini, J. Q. Quach, M. Polini, and G. M. Andolina, Rev. Mod. Phys. **96**, 031001 (2024).
- [11] S. Julià-Farré, T. Salamon, A. Riera, M. N. Bera, and M. Lewenstein, Phys. Rev. Res. **2**, 023113 (2020).
- [12] G. M. Andolina, D. Farina, A. Mari, V. Pellegrini, V. Giovannetti, and M. Polini, Phys. Rev. B **98**, 205423 (2018).
- [13] D. Rossini, G. M. Andolina, D. Rosa, M. Carrega, and M. Polini, Phys. Rev. Lett. **125**, 236402 (2020).
- [14] A. Lunkin, A. Kitaev, and M. Feigel’man, Physical Review Letters **125**, 196602 (2020).
- [15] A. M. García-García, B. Loureiro, A. Romero-Bermúdez, and M. Tezuka, Physical Review Letters **120**, 241603 (2018).
- [16] C. Liu, X. Chen, and L. Balents, Physical Review B **97**, 245126 (2018).
- [17] Y. Huang, Y. Tan, and N. Y. Yao, (2024), 10.48550/arXiv.2409.07043.
- [18] W. Fu and S. Sachdev, Physical Review B **94**, 035135 (2016).
- [19] P. Zhang, Frontiers of Physics **17**, 43201 (2022).
- [20] J. S. Cotler, G. Gur-Ari, M. Hanada, J. Polchinski, P. Saad, S. H. Shenker, D. Stanford, A. Streicher, and M. Tezuka, Journal of High Energy Physics **2017**, 118 (2017).
- [21] V. Veitch, S. A. Hamed Mousavian, D. Gottesman, and J. Emerson, New Journal of Physics **16**, 013009 (2014).
- [22] P. W. Shor, Physical Review A **52**, R2493–R2496 (1995).
- [23] A. R. Calderbank and P. W. Shor, Physical Review A **54**, 1098–1105 (1996).
- [24] C. H. Bennett, D. P. DiVincenzo, J. A. Smolin, and W. K. Wootters, Physical Review A **54**, 3824–3851 (1996).
- [25] E. Knill and R. Laflamme, Physical Review A **55**, 900–911 (1997).
- [26] D. Gottesman, (1997), 10.48550/arXiv.quant-ph/9705052.
- [27] P. W. Shor, “Proceedings of 37th conference on foundations of computer science,” (1996).
- [28] D. Gottesman, Physical Review A **57**, 127–137 (1998).
- [29] A. Y. Kitaev, Annals of Physics **303**, 2–30 (2003).
- [30] E. T. Campbell, B. M. Terhal, and C. Vuillot, Nature **549**, 172–179 (2017).
- [31] L. Leone, S. F. Oliviero, and A. Hamma, Physical Review Letters **128**, 050402 (2022).
- [32] C. E. P. Robin and M. J. Savage, (2024), 10.48550/arXiv.2405.10268.

- [33] F. Brökemeier, S. M. Hengstenberg, J. W. T. Keeble, C. E. P. Robin, F. Rocco, and M. J. Savage, (2024), 10.48550/arXiv.2409.12064.
- [34] I. Chernyshev, C. E. P. Robin, and M. J. Savage, (2024), 10.48550/arXiv.2411.04203.
- [35] C. Cao, G. Cheng, A. Hamma, L. Leone, W. Munizzi, and S. F. E. Oliviero, (2024), 10.48550/arXiv.2403.07056.
- [36] S. F. E. Oliviero, L. Leone, and A. Hamma, *Physical Review A* **106**, 042426 (2022).
- [37] C. D. White, C. Cao, and B. Swingle, *Physical Review B* **103**, 075145 (2021).
- [38] R. Nyström, N. Pranzini, and E. Keski-Vakkuri, (2024), 10.48550/arXiv.2409.11473.
- [39] S. Cepollaro, S. Cusumano, A. Hamma, G. L. Giudice, and J. Odavic, (2025), 10.48550/arXiv.2412.11918.
- [40] L. Leone, S. F. E. Oliviero, Y. Zhou, and A. Hamma, *Quantum* **5**, 453 (2021).
- [41] S. F. E. Oliviero, L. Leone, and A. Hamma, *Physics Letters A* **418**, 127721 (2021).
- [42] Z.-C. Yang, C. Chamon, A. Hamma, and E. R. Mucciolo, *Physical Review Letters* **115**, 267206 (2015).
- [43] S. Zhou, Z. Yang, A. Hamma, and C. Chamon, *SciPost Physics* **9**, 087 (2020).
- [44] A. Russomanno, G. Passarelli, D. Rossini, and P. Lucignano, (2025), 10.48550/arXiv.2502.01431.
- [45] Z.-C. Yang, A. Hamma, S. M. Giampaolo, E. R. Mucciolo, and C. Chamon, *Physical Review B* **96**, 020408 (2017).
- [46] M. Rigol, V. Dunjko, and M. Olshanii, *Nature* **452**, 854–858 (2008).
- [47] A. Pal and D. A. Huse, *Physical Review B* **82**, 174411 (2010).
- [48] R. Nandkishore and D. A. Huse, *Annual Review of Condensed Matter Physics* **6**, 15–38 (2015).
- [49] C. Chamon, A. Hamma, and E. R. Mucciolo, *Physical Review Letters* **112**, 240501 (2014).
- [50] D. Shaffer, C. Chamon, A. Hamma, and E. R. Mucciolo, *Journal of Statistical Mechanics: Theory and Experiment* **2014**, P12007 (2014).
- [51] P. H. C. Lau, C.-T. Ma, J. Murugan, and M. Tezuka, *Physics Letters B* **795**, 230–235 (2019).
- [52] A. Kitaev, in *Proceedings of the Stanford SITP seminars* (2014).
- [53] B. Kobrin, Z. Yang, G. D. Kahanamoku-Meyer, C. T. O’lund, J. E. Moore, D. Stanford, and N. Y. Yao, *Physical Review Letters* **126**, 030602 (2021).
- [54] P. Orman, H. Gharibyan, and J. Preskill, (2024), 10.48550/arXiv.2403.13884.
- [55] K. Adhikari and A. Bose, (2018), 10.48550/arXiv.1807.07240, arXiv:1807.07240 [math].
- [56] P. J. Forrester, *Journal of Physics A: Mathematical and General* **39**, 6861 (2006).
- [57] P. J. Forrester, J. R. Ipsen, and S. Kumar, (2017), 10.48550/arXiv.1708.00967, arXiv:1708.00967 [math-ph].
- [58] K. Zyczkowski and H.-J. Sommers, *Journal of Physics A: Mathematical and General* **33**, 2045 (2000).
- [59] S. B. Bravyi and A. Y. Kitaev, *Annals of Physics* **298**, 210–226 (2002).
- [60] P. H. Chris Lau, C.-T. Ma, J. Murugan, and M. Tezuka, *Journal of Physics A: Mathematical and Theoretical* **54**, 095401 (2021).
- [61] P. Lydžba, M. Rigol, and L. Vidmar, *Physical Review Letters* **125**, 180604 (2020).
- [62] Y. Huang and Y. Gu, *Physical Review D* **100**, 041901 (2019).
- [63] P. Zhang, C. Liu, and X. Chen, *SciPost Physics* **8**, 094 (2020).
- [64] D. N. Page, *Physical Review Letters* **71**, 1291–1294 (1993).
- [65] J. Odavić, M. Viscardi, and A. Hamma, (2025), 10.48550/arXiv.2412.10228.
- [66] We consider N bipartitions as a representative sample from the $\binom{N/2}{N/4}$ possible bipartitions.
- [67] B. Jasser, J. Odavić, and A. Hamma, “Appendices/supplementary material for “stabilizer entropy and entanglement complexity in the sachdev-ye-kitaev model”,” (2025).
- [68] W. Mück, *Physical Review D* **109**, 126001 (2024).
- [69] S. True and A. Hamma, *Quantum* **6**, 818 (2022).
- [70] J. Odavić, G. Torre, N. Mijić, D. Davidović, F. Franchini, and S. M. Giampaolo, *Quantum* **7**, 1115 (2023).
- [71] J. Odavić and P. Mali, *Journal of Statistical Mechanics: Theory and Experiment* **2021**, 043204 (2021).
- [72] Y. Y. Atas, E. Bogomolny, O. Giraud, and G. Roux, *Physical Review Letters* **110**, 084101 (2013).
- [73] S. Bravyi and A. Kitaev, *Physical Review A* **71**, 022316 (2005).
- [74] L. Leone and L. Bittel, *Physical Review A* **110**, L040403 (2024).
- [75] P. Niroula, C. D. White, Q. Wang, S. Johri, D. Zhu, C. Monroe, C. Noel, and M. J. Gullans, *Nature Physics* **20**, 1786–1792 (2024).
- [76] T. Haug and L. Piroli, *Physical Review B* **107**, 035148 (2023).
- [77] G. Lami and M. Collura, *Physical Review Letters* **131**, 180401 (2023).
- [78] M. Collura, J. D. Nardis, V. Alba, and G. Lami, (2025), 10.48550/arXiv.2412.05367.
- [79] A. M. García-García and J. J. Verbaarschot, *Physical Review D* **94**, 126010 (2016).
- [80] A. G. Catalano, J. Odavić, G. Torre, A. Hamma, F. Franchini, and S. M. Giampaolo, (2024), 10.48550/arXiv.2406.19457.
- [81] Z.-W. Liu and A. Winter, *PRX Quantum* **3**, 020333 (2022).
- [82] X. Turkesi, A. Dymarsky, and P. Sierant, (2025), 10.48550/arXiv.2312.11631.
- [83] A. Hamma, R. Ionicioiu, and P. Zanardi, *Physical Review A* **71**, 022315 (2005).
- [84] E. Tirrito, P. S. Tarabunga, G. Lami, T. Chanda, L. Leone, S. F. E. Oliviero, M. Dalmonte, M. Collura, and A. Hamma, *Physical Review A* **109**, L040401 (2024).
- [85] X. Dong, A. Lewkowycz, and M. Rangamani, *Journal of High Energy Physics* **2016**, 28 (2016).
- [86] H. Yao and X.-L. Qi, *Physical Review Letters* **105**, 080501 (2010).
- [87] J. Schliemann, *Physical Review B* **83**, 115322 (2011).
- [88] J. de Boer, J. Järvelä, and E. Keski-Vakkuri, *Physical Review D* **99**, 066012 (2019).
- [89] K. Okuyama, *Physics Letters B* **820**, 136600 (2021).
- [90] B. Bhattacharjee, P. Nandy, and T. Pathak, *Physical Review B* **104**, 214306 (2021).
- [91] G. Styliaris, N. Anand, and P. Zanardi, *Physical Review Letters* **126**, 030601 (2021).
- [92] R. Alicki and M. Fannes, *Phys. Rev. E* **87**, 042123 (2013).
- [93] F. Caravelli, G. Coulter-De Wit, L. P. García-Pintos,

and A. Hamma, Phys. Rev. Res. **2**, 023095 (2020).
 [94] F. Caravelli, B. Yan, L. P. García-Pintos, and
 A. Hamma, Quantum **5**, 505 (2021).

[95] L. P. García-Pintos, A. Hamma, and A. del Campo,
 Phys. Rev. Lett. **125**, 040601 (2020).

Appendix A: On the evaluation of Stabilizer Rényi Entropy

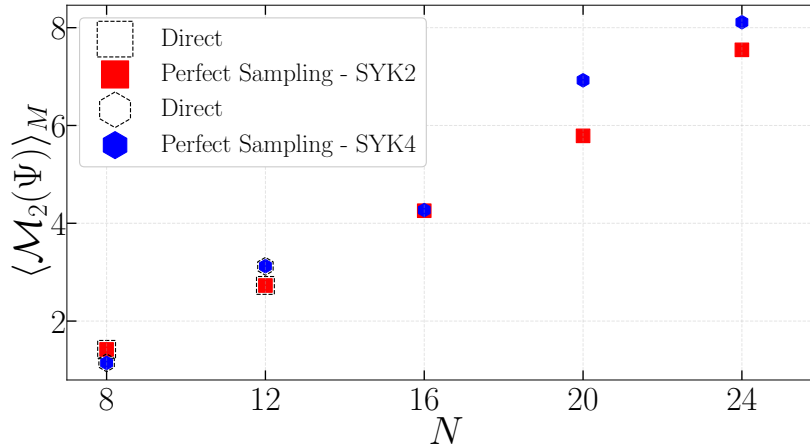


Figure 7: This figure shows the ability of the Perfect Sampling algorithm to evaluate the SRE efficiently. We use $M = 100$ different disorder realizations to compute the average SRE and perform an average (denoted in the y -label as $\langle \bullet \rangle_M$) over these realizations. We observe that for larger systems, the SYK-4 model host more magic as compared to the SYK-2 model. The coupling strength in general is set $J = 1$.

Here, we outline key details of the Perfect Sampling algorithm [1, 2], essential for obtaining reliable estimates of the Stabilizer Rényi Entropy (SRE) presented in Fig. 5. Starting from a state vector supported on $N/2$ qubits (where N denotes the number of Majorana fermions) obtained via exact diagonalization, we represent it as a Matrix Product State (MPS) with a maximum bond dimension of $\chi = 2^{N/2}$ and a truncation cutoff of 10^{-8} using the ITensor library [3, 4]. We then sample 10^4 Pauli strings, leading to an absolute error in the stabilizer entropy estimation within the range $10^{-1} - 10^{-2}$.

To verify the accuracy of this approach, we consider smaller system sizes in Fig. 7, where the SRE can be computed exactly from the state vector, evaluating all the 4^N expectation values of the Pauli strings, confirming that the method achieves sufficient precision. A similar approach was employed in [5]. The open-source ITensor implementation of this method will be made available in a forthcoming publication [6].

In Fig. 5 (b) the green crosses are related to sizes such that $N \bmod 8 = 0$, for which the fit parameters are $a = 0.57, b = 0.036$, blue crosses for $N \bmod 8 = 2, 6$, with $a = 0.44, b = 0.09$, and red circles for $N \bmod 8 = 4$, with $a = 0.46, b = 0.07$. The lines represent fits to the function $f(x) = a(1 - \exp(-bx))$.

In Fig. 5(c), we highlight a factorizable n -qubit state with the maximal amount of single-qubit magic, shown in magenta. It is known that there is a single qubit state which maximizes the SRE, the golden state $|G\rangle\langle G| = \frac{1}{2} \left(I + \frac{X+Y+Z}{\sqrt{3}} \right)$. The stabilizer entropy of its n -qubits product state is $\mathcal{M}_2(|G\rangle\langle G|^{\otimes n}) = n \log_2 \left(\frac{3}{2} \right)$.

Appendix B: Capacity of entanglement - quick rederivation

For the convenience of the reader, we compute here Eq. 16 for the pure Haar random states. Original derivations were performed in [7, 8]. For Haar random pure states, the average Rényi entropy to leading order in N , with positive integer α , is given by

$$S_\alpha^{\text{Haar}} = \frac{1}{1-\alpha} \log \left[2^{N-R(1+\alpha)} \sum_{k=1}^{\alpha} H(\alpha, k) 2^{(2R-N)k} \right] \quad (\text{B1})$$

where the coefficients $H(\alpha, k) = \frac{1}{\alpha} \binom{\alpha}{k} \binom{\alpha}{k-1}$ are known as Narayana numbers. To start the calculation we simplify the expression first by fixing the system-to-subsystem size ratio to $R/N = 1/2$ to obtain for Eq. (B1) the following

$$S_{\alpha}^{\text{Haar}} = \frac{1}{1-\alpha} \log \left[2^{\frac{N}{2}(1-\alpha)} \sum_{k=1}^{\alpha} H(\alpha, k) \right]. \quad (\text{B2})$$

Plugging this expression into the expression for modular entropy we obtain

$$\tilde{S}_{\alpha}^{\text{Haar}} = -\alpha H_{\alpha-\frac{1}{2}} + \alpha H_{\alpha+1} + \frac{1}{2}(\alpha(N-4)\log(2) - \log(\pi)) + \log \left(\frac{2^{\frac{1}{2}(-\alpha L+4\alpha+L)} \Gamma(\alpha + \frac{1}{2})}{\Gamma(\alpha+2)} \right), \quad (\text{B3})$$

where $H_x = \sum_{k=1}^x \frac{1}{k}$ is the Harmonic functions and $\Gamma(x)$ are the usual gamma functions. After taking another derivative yields closed form the expression for the capacity of entanglement

$$\partial_{\alpha} \tilde{S}_{\alpha}^{\text{Haar}} = \alpha \left(\Psi(\alpha+2) - \Psi\left(\alpha + \frac{1}{2}\right) \right), \quad (\text{B4})$$

where $\Psi = \partial_{\alpha} \log(\Gamma(\alpha))$ is the derivative of the logarithm of the Gamma function, known also as the digamma function. Evaluating this function at $\alpha = 1$ we obtain

$$\partial_{\alpha} \tilde{S}_{\alpha}^{\text{Haar}} \Big|_{\alpha=1} = \frac{11}{4} - \frac{\pi^2}{3} \approx -0.539868, \quad (\text{B5})$$

to leading order in system size. Notice that this result does not explicitly depend on the system size. Numerical checks against synthetic Haar states for finite sizes (up to 20 qubits) confirm this estimate.

Appendix C: Ensemble realizations

Throughout our work, we generate M independent realizations of the SYK-4 and SYK-2 Hamiltonians which we scale (multiply) by the scalar parameter g . This method is particularly advantageous for larger system sizes, where constructing the SYK-4 Hamiltonian becomes computationally expensive and represents the main computational bottleneck. Even though the Hamiltonian is sparse, it requires significant resources to store, e.g. for $N = 32$ a single sparse realization of the SYK4 Hamiltonian takes up around 1GB of memory. The step size for the interpolation parameter used through the text $\Delta g = 1/100$, while exclusively for the SRE computation to ease the computation load we compute it for every $\Delta g = 0.05$. The number of realizations for each fermion number N is as follows: $N = 6$ (1000), $N = 8$ (1000), $N = 10$ (1000), $N = 12$ (400), $N = 14$ (400), $N = 16$ (200), $N = 18$ (200), $N = 20$ (200), $N = 22$ (100), $N = 24$ (100), $N = 26$ (100), $N = 28$ (50), $N = 30$ (30), and $N = 32$ (10).

Appendix D: Analytical derivation of the logarithmic anti-flatness for the SYK-2 model

Here we provide some important details enabling and leading to the closed-form expression in Eq. (14). We closely follow the derivation performed for $\alpha = 2$ Rényi entropy in Ref. [9, 10]. In particular, starting from Eq.(23) in [9] we have for the $\alpha = 3$ that

$$S_R^{(3)} = -\frac{1}{2} \sum_{k=1}^R \ln [\lambda_k^3 + (1 - \lambda_k)^3], \quad (\text{D1})$$

where $\{\lambda_k; k = 1, 2, \dots, R\}$ are the eigenvalues of the reduced density matrix. After tracing out degrees of freedom, the subscript R -th is a notation used to specify the one-body correlation (or reduced density) matrix ρ_R . The key insight in deriving $\alpha = 2$ was the observation in Ref. [10] that the SYK2 model subsystem eigenvalues belong to the β -Jacobi ensemble with $\beta = 2$. In particular, subsystem reduced density matrix eigenvalues, for different relative size f , have the following form

$$\mathcal{F}(f, p) = \frac{1}{2\pi f} \frac{\sqrt{p(1-p) + f(1-f) - \frac{1}{4}}}{p(1-p)}, \quad (\text{D2})$$

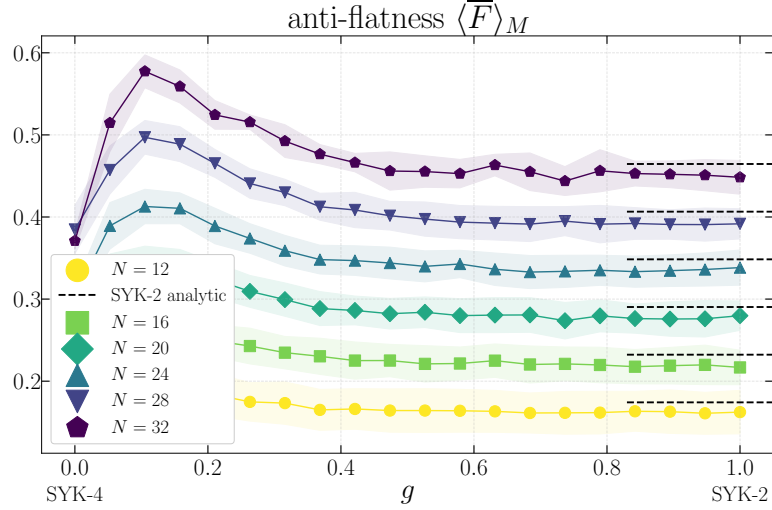


Figure 8: Ensemble averaged half-system ($f = 1/2$) anti-flatness in the ground states of the interpolated SYK model. The overline also indicates an average has been taken over the N possible bipartitions. The shaded areas represent the standard deviation across M realizations of the Hamiltonian. The dashed lines are the analytical results given in Eq. (D9).

where we note that this PDF is supported only on the domain $p \in [p_-, p_+]$, with $p_{\pm} = \frac{1}{2} \pm \sqrt{f(1-f)}$. The average third Rényi entropy is obtained by

$$\overline{S}^{(3)} = -\frac{R}{2} \int dp \mathcal{F}(f, p) \ln [p_i^3 + (1-p_i)^3], \quad (\text{D3})$$

after replacing the sum in Eq. (D1) as $\sum_i \rightarrow R \int dp F(f, p)$. We therefore have

$$\overline{S}^{(3)} = -\frac{R}{4\pi f} \int \frac{\sqrt{p(1-p) + f(1-f)} - \frac{1}{4}}{p(1-p)} \ln [p_i^3 + (1-p_i)^3] \quad (\text{D4})$$

Changing the variable as $p = (\lambda + 1)/2$ we obtain

$$\overline{S}^{(3)} = -\frac{R}{2\pi f} \int_{\lambda_-}^{\lambda_+} \frac{\sqrt{\frac{1-\lambda^2}{4} + f(1-f)} - \frac{1}{4}}{1-\lambda^2} \ln \left[\left(\frac{\lambda+1}{2} \right)^3 + \left(1 - \frac{\lambda+1}{2} \right)^3 \right] d\lambda, \quad (\text{D5})$$

where the term in the logarithm after expanding, simplifying, and rearranging reads

$$\ln \left[\left(\frac{\lambda+1}{2} \right)^3 + \left(1 - \frac{\lambda+1}{2} \right)^3 \right] = -\sum_{n=1}^{\infty} \frac{1}{n} \left(\frac{3}{4} \right)^n (1-\lambda^2)^n \quad (\text{D6})$$

Where we expanded the logarithm as $\ln(1-x) = -\sum_{n=1}^{\infty} \frac{x^n}{n}$ leading to

$$\overline{S}^{(3)} = \frac{R}{4\pi f} \sum_{n=1}^{\infty} \frac{1}{n} \left(\frac{3}{4} \right)^n \underbrace{\int_{-2\sqrt{f(1-f)}}^{+2\sqrt{f(1-f)}} \frac{\sqrt{(1-\lambda^2) + 4f(1-f)} - 1}{1-\lambda^2} (1-\lambda^2)^n d\lambda}_{-2(f-1)f\pi_2 F_1\left(\frac{1}{2}, 1-n, 2, -4(f-1)f\right)}. \quad (\text{D7})$$

Using the following definition of the logarithmic anti-flatness

$$F = 2(S_2(\psi_R) - S_3(\psi_R)), \quad (\text{D8})$$

we trivially obtain

$$\bar{F}(R, f) = 2R(1-f) \sum_{n=1}^{\infty} \frac{1}{n} \left(\frac{1}{2^n} - \frac{1}{2} \frac{3^n}{4^n} \right) {}_2F_1 \left(\frac{1}{2}, 1-n, 2, 4f(1-f) \right), \quad (\text{D9})$$

In Fig. 8 we showcase the validity of the derived expression for the SYK-2 model.

Appendix E: Hamiltonian spectral statistics

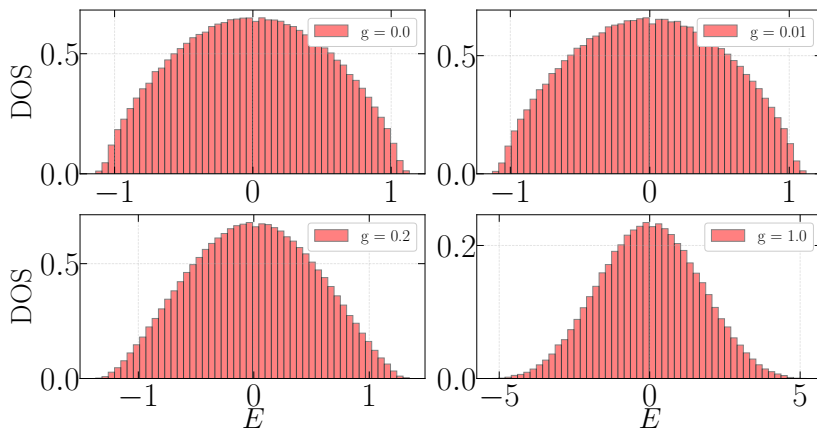


Figure 9: Density of states (DOS) of the H_g spectrum for $N = 22$ fermions with support on 11 qubits, with $M = 40$ realizations of the disordered Hamiltonian. We considered 40960 eigenvalues for each panel and corresponding g . See text for details and discussions. An interesting observation regarding the DOS support is highlighted below.

Here we discuss the nuances related to the Hamiltonian spectrum of the interpolated model H_g . We first expose the results related to the full Hamiltonian spectrum of the model. More specifically, we plot the Density of states (DOS) of the spectrum in Fig. 9. We can infer that its shape is akin to the one encountered in Gaussian ensembles of Random Matrix Theory (RMT) and that of Wigner semi-circle distribution. To study universal features of a system, it is essential to look at the gaps between eigenvalues rather than the eigenvalues distribution itself, that is not universal. A more detailed analysis of eigenvalues gaps of the SYK4 across different system sizes can be found in [11]. The SYK4 model admits different universality classes due to the existence of a particular size-dependent particle-hole symmetry of Gaussian ensembles as tabulated in table I. While the bulk spectrum of the SYK4 model does indeed behave according to RMT [12], the spectrum at the edges is a subject of current research [13].

N	16	18	20	22	24	26	28	30	32
class	GOE	GUE	GSE	GUE	GOE	GUE	GSE	GUE	GOE

Table I: Due to a particular particle-hole symmetry, the SYK-4 model exhibits all three Gaussian ensembles [11].

In Fig. 9, by changing the interpolation parameter $g \in [0, 1]$ we infer a smooth transition from a semi-circle type DOS ($g \ll 1$) to one that of a Gaussian (as g approaches 1), final lower right panel [14]. Note that we take into account every second eigenvalue since SYK4 spectrum eigenvalues are all twice degenerate. For consistency, we extend this choice of forming the DOS from every second eigenvalue for all values of g . Therefore the total number of eigenvalues considered for each panel of Fig. 9 is $M2^{\frac{N}{2}-1} = 40960$.

We highlight a noteworthy aspect of the smooth change between the SYK4 and SYK2 DOS that can not be directly observed in Fig. 9. More specifically, for small values of g in the range $g \in [0, 0.1]$, we observe the shrinking of the energy support of the Hamiltonian eigenvalues and correspondingly the DOS support. We make this observation for all system sizes up to $N = 22$ for which we computed the full spectrum. For values of g that are larger than 0.1, the support grows and the DOS starts spreading rather than shrinking. This change in behavior in the DOS could be related to our observations presented in Ref. 3 for the ground state. Interestingly, the ground state properties are sensitive to these changes in the Hamiltonian behavior, while the middle of the spectrum states are

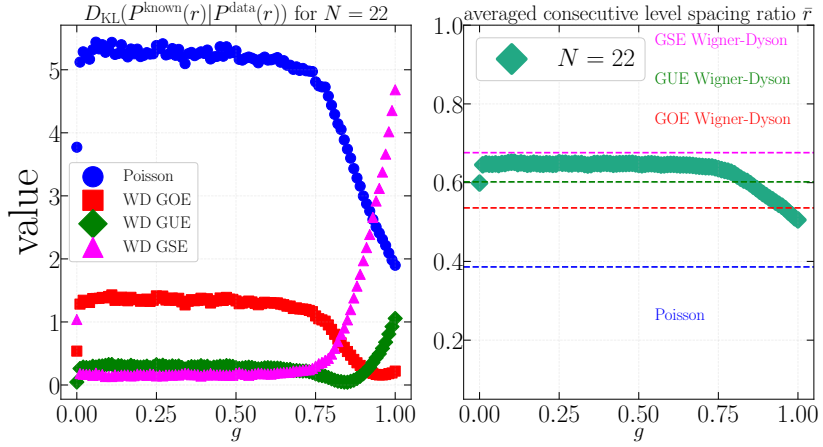


Figure 10: Spectral statistics results. *Left panel*: KL divergence (defined in the main text) between known Gaussian ensemble RMT distributions and the underlying dataset for the consecutive gap ratios PDF $P(r)$. *Right panel*: The averaged consecutive gap ratios. We considered 40960 eigenvalues for each panel and corresponding g . Smaller systems size exhibit similar findings to the presented results for $N = 22$ in this figure.

not. This phenomenology can potentially be related to the findings in [15] regarding the low-temperature behavior of the interpolated SYK model.

To round off our short survey into the Hamiltonian spectrum we present Fig 10. In the left panel, we show the results for the KL divergence (defined in the main text) between the full Hamiltonian H_g spectral statistics as compared to the well-known Gaussian RMT ensembles. The result indicates that for most values of the interpolation parameter g the underlying spacing distributions are similar to the correlated Wigner-Dyson (WD) RMT ensemble expectations. However, we note that at around $g \sim 0.75$ there is a change of behavior toward the uncorrelated Poisson distribution which we further comment on below. The explicit expressions of the distribution of consecutive gap ratios have been derived in [16], but for the convenience of the reader we present them below. For the standard correlated ensembles (GOE, GUE, and GSE, with $\beta = 1, 2, 4$ respectively) we have

$$P^{\text{WD}}(r, \beta) = \frac{Z_\beta^{-1} \cdot (r + r^2)^\beta}{(1 + r + r^2)^{1 + \frac{3}{2}\beta}}, \quad (\text{E1})$$

where

$$Z_\beta = \begin{cases} \frac{8}{27}, & \beta = 1, \\ \frac{4}{81} \cdot \frac{\pi}{\sqrt{3}}, & \beta = 2, \\ \frac{4}{729} \cdot \frac{\pi}{\sqrt{3}}, & \beta = 4, \end{cases} \quad (\text{E2})$$

while the uncorrelated ensembles typically follow the Poisson distribution, which in terms of the consecutive gap ratios reads

$$P^{\text{Poisson}}(r) = \frac{1}{(1 + r)^2}. \quad (\text{E3})$$

We associate consistent color coding between all figures in this work, we choose blue for the Poisson distribution, red for GOE, green for GUE and magenta for GSE.

In the right panel of Fig 10 we perform a complementary analysis of the average consecutive gap ratios, defined as

$$\bar{r} = \left\langle \left\langle \frac{\min(s_{k,j}, s_{k+1,j})}{\max(s_{k,j}, s_{k+1,j})} \right\rangle \right\rangle_{2^{N/2-1}-2, M} = \frac{1}{M(2^{N/2-1} - 2)} \sum_{j=1}^M \sum_{k=1}^{2^{N/2-1}-2} \frac{\min(s_{k,j}, s_{k+1,j})}{\max(s_{k,j}, s_{k+1,j})} \quad (\text{E4})$$

where $s_{k,j} = \lambda_{k+1,j} - \lambda_{k,j}$, and the index $j = 1, 2, \dots, M$ runs over M available realizations while the k index the available eigenvalues. It is known [16] that the WD ratios

$$\bar{r}^{\text{WD-GOE}} = 4 - 2\sqrt{3} \approx 0.53590, \quad (\text{E5})$$

$$\bar{r}^{\text{WD-GUE}} = 2\frac{\sqrt{3}}{\pi} - \frac{1}{2} \approx 0.60266, \quad (\text{E6})$$

$$\bar{r}^{\text{WD-GSE}} = \frac{32\sqrt{3}}{15\pi} - \frac{1}{2} \approx 0.67617, \quad (\text{E7})$$

while for the uncorrelated ensemble, we have

$$\bar{r}^{\text{Poisson}} = 2 \ln 2 - 1 \approx 0.38629. \quad (\text{E8})$$

We observe that indeed for the system size considered ($N = 22$, but similar follows for other smaller system sizes), we recover universal statistics of the GUE for the SYK4 ($g = 0$) model that matches the GUE ensemble as previously shown in [11] and in agreement to Table I. Interestingly, as soon as we introduce finite g the underlying distribution of the consecutive level spacing statistics changes its universality class, and more agreement is found with the GSE ensemble compared to the other distributions. This is potentially related to the fine-tuned nature of the SYK4 model and to the particle-hole symmetry that is lost at any non-vanishing g . Similar observation on the quantum chaotic nature of the Hamiltonian spectrum for $N \leq 22$ for all choices of the interpolation parameter has been highlighted in [12]. However, we underline that the analysis performed by the authors of [12] put the focus on the bulk spectrum, which can influence the overall value of the average gap.

Moreover, we observe that the full Hamiltonian spectrum manifestly conforms to the universal correlated statistics of RMT until around $g \approx 0.75$ where more similarity can be found with the uncorrelated Poisson distribution (left panel). However, we note that this type of analysis is influenced by the binning of the PDF and the finite-size effects that naturally plague any finite quantum many-body system. Overall this stops us from providing conclusive judgment on the chaoticity/integrability present in the model from the full Hamiltonian spectrum. In a way, this justifies our approach to studying state complexity instead as has been done in the main text.

In the next subsection on Entanglement Spectrum Statistics, we comment on some features that some surprising SYK model features are inherited by the eigenstates and are not restricted only to the eigenvalues.

Appendix F: Analysis of the gap

A comment on the behavior of the gap between the ground state and the first excited state in the interpolated SYK model is in order. In quantum many-body systems, the behavior of the energy gap is instrumental in understanding quantum phase transitions [18]. Therefore, it is of value if one can infer a transition between the complex SYK4 and integrable SYK2 phase based on this commonly studied observable in quantum systems.

The low energy spectrum of the interpolated SYK model behaves differently between the SYK4 ($g = 0$) and SYK2 $g = 1$ models. Individual energy levels have the spacing $\sim \exp(-NS)$ with S being the system's entropy as $N \rightarrow \infty$ for the SYK4 model, while for the SYK2 the spacing behaves as $\sim 1/N$ at the bottom of the band [17].

In Fig. 11, we show the behavior of the average ground state to the first excited state gap for different choices of the interpolation parameter g . Fitting a power law function to the data we observe consistency with the expected N^{-1} power law with exponent -1 as g approaches 1. On the other hand, when we approach the SYK4 point, i.e. g going to 0, we are still able to fit a power law function with reasonable precision. This implies that for the finite system data, it is hard to differentiate between a power-law and the exponential behavior expected for the SYK4 model, indicating the ineffectiveness of this particular probe.

Appendix G: Entanglement Spectral Statistics (ESS) and normalized Reduced Density Matrix (RDM) spectrum

In this section, we complete our survey of the ESS of the middle spectrum state not presented in the main text. More specifically, we repeat the same analysis presented in Fig. 4, but for the middle of the spectrum state (MS) at $E \sim 0$, see Fig. 9. In Fig. 12, we observe that for the considered system sizes the ESS does not show agreement with RMT universal ensembles and shows good agreement with the uncorrelated Poisson distribution.

In Fig. 13, we expand on this point and demonstrate a broader view-point of the absence of universal behavior in the RDM eigenvalues. In the top panel, we show the results for pure Haar random states on $N = 11$ qubits.

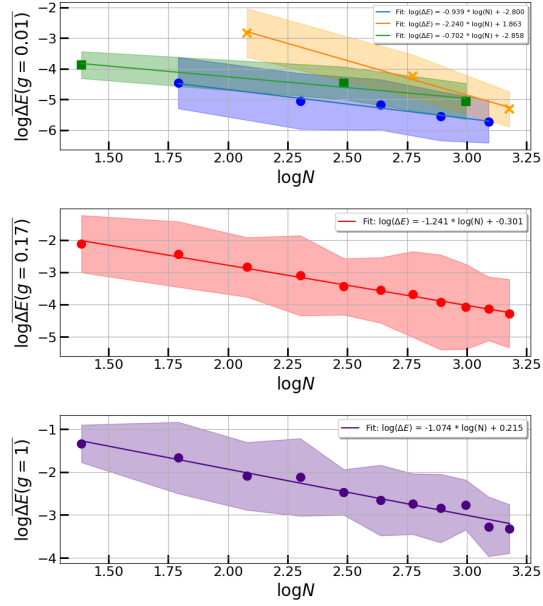


Figure 11: Power-law fits of the GSs energy gaps $\Delta E = E_1 - E_0$ of H_g for different values of the interpolation parameter g , where E_0 is the GS energy and E_1 the first excited state energy. As soon as g deviates from zero, the low-temperature density of states no longer follows an exponential distribution [17]. The first plot, corresponding to $g = 0.01$, shows three distinct fits, reflecting a remnant of the symmetry in the model at $g = 0$, see [11]. The orange line corresponds to GOE, the blue one to GSE and the red line to the GUE. Each data point represents an average over 100 disorder realizations for system sizes smaller than 20, and 20 disorder realizations for larger sizes.

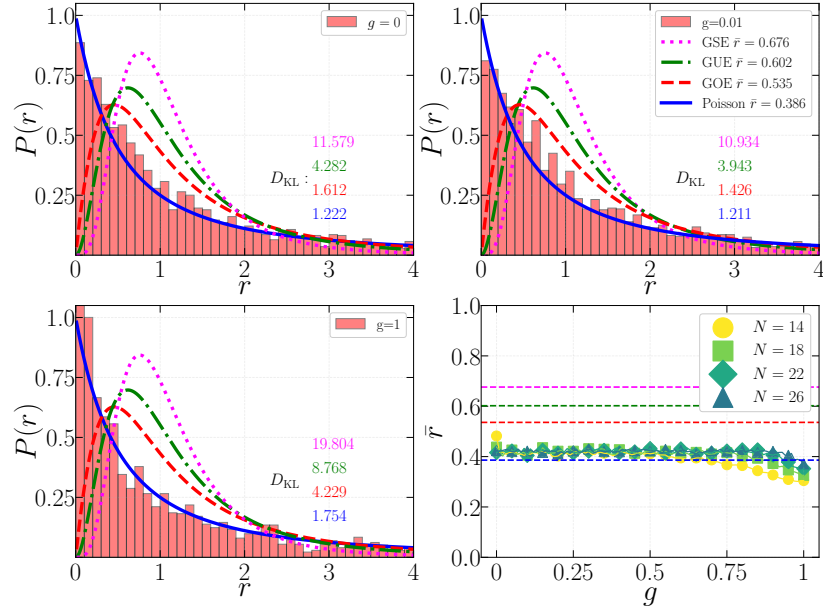


Figure 12: ESS of the middle of spectrum state RDM eigenvalues of the H_g model for different values of g . We superimpose the analytical curves for the Wigner-Dyson (dashed) and Poisson (blue continuous) distribution for comparison. System size $N = 22$ and number of realizations is $M = 100$. The number of bins used for the histogram is 100. The colored numbers represent the KL divergence of data against known distributions [16]

To generate such states we simply draw real and imaginary parts of the expansion coefficients of $|\psi\rangle$ as random Gaussian variables, and normalize the output vector state [19]. This procedure provides an excellent agreement with the predicted Marchenko-Pasture (M-P) distribution defined in the main text and represented with the purple line

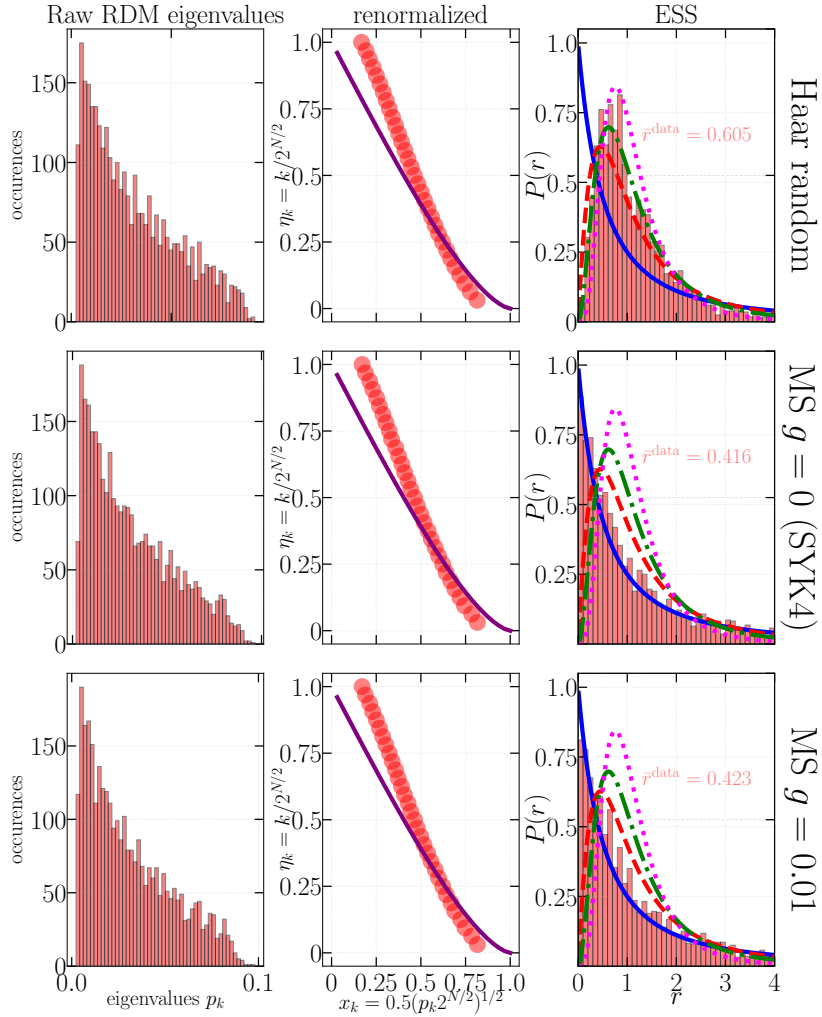


Figure 13: Haar vs middle of the spectrum (MS) SYK states comparative analysis across a single bipartition (same results for other bipartitions). *Upper row*: Haar states included by influenced by the odd/even effects (the reason for the mismatch with the purple M-P distribution [20]); *Middle row*: MS state for the $g = 0$ SYK4 Hamiltonian; *Lower row*: MS state for $g = 0.01$. Other parameters: number of realization $M = 100$, nb of spins $N = 11$ (fermions $N = 22$) and across bipartition $[1, 2, 3, 4, 5]$.

in the middle panels. We note that the disagreement between obtained values and the M-P distribution comes from the odd/even effect that vanishes in the thermodynamic limit. The final panel of the upper row shows that ESS for the Haar states does conform with the RMT prediction and universal GUE ensemble. The Haar example serves as a reference point to the results we obtain for the MS state of the interpolated model. More specifically, we can observe that the RDM spectrum itself shows quite similar features to that of a Haar random state, however, the ESS point to an uncorrelated ensemble and the non-universal Poisson distribution. These unorthodox features of SYK4 and of the interpolated model, when it comes to universality statistics probes, are most likely part of the broader context of the particular structure that the eigenstates entail and are evidenced already in the above mentioned chapter on the Hamiltonian spectrum statistics.

-
- [1] T. Haug and L. Piroli, Physical Review B **107**, 035148 (2023).
 - [2] G. Lami and M. Collura, Physical Review Letters **131**, 180401 (2023).
 - [3] M. Fishman, S. White, and E. M. Stoudenmire, SciPost Physics Codebases , 004 (2022).
 - [4] M. Fishman, S. White, and E. M. Stoudenmire, SciPost Physics Codebases , 004 (2022).
 - [5] J. Odavić, M. Viscardi, and A. Hamma, (2025), 10.48550/arXiv.2412.10228.

- [6] M. Viscardi, J. Odavic, and A. Hamma, To appear.
- [7] J. de Boer, J. Järvelä, and E. Keski-Vakkuri, *Physical Review D* **99**, 066012 (2019).
- [8] K. Okuyama, *Physics Letters B* **820**, 136600 (2021).
- [9] P. Lydzba, M. Rigol, and L. Vidmar, *Physical Review B* **103**, 104206 (2021).
- [10] C. Liu, X. Chen, and L. Balents, *Physical Review B* **97**, 245126 (2018).
- [11] J. S. Cotler, G. Gur-Ari, M. Hanada, J. Polchinski, P. Saad, S. H. Shenker, D. Stanford, A. Streicher, and M. Tezuka, *Journal of High Energy Physics* **2017**, 118 (2017).
- [12] A. M. García-García, B. Loureiro, A. Romero-Bermúdez, and M. Tezuka, *Physical Review Letters* **120**, 241603 (2018).
- [13] A. Altland, K. W. Kim, T. Micklitz, M. Rezaei, J. Sonner, and J. J. M. Verbaarschot, *Physical Review Research* **6**, 033286 (2024).
- [14] G. Sarosi, “*Ads₂ holography and the syk model*,” in *Proceedings of XIII Modave Summer School in Mathematical Physics — PoS(Modave2017)*, Vol. 323 (SISSA Medialab, 2018) p. 001.
- [15] A. Lunkin, A. Kitaev, and M. Feigel’man, *Physical Review Letters* **125**, 196602 (2020).
- [16] Y. Y. Atas, E. Bogomolny, O. Giraud, and G. Roux, *Physical Review Letters* **110**, 084101 (2013).
- [17] D. Chowdhury, A. Georges, O. Parcollet, and S. Sachdev, *Reviews of Modern Physics* **94**, 035004 (2022).
- [18] S. Sachdev, *Quantum Phase Transitions* (Cambridge University Press, 2011).
- [19] K. Zyczkowski and H.-J. Sommers, *Journal of Physics A: Mathematical and General* **33**, 2045 (2000).
- [20] Z.-C. Yang, C. Chamon, A. Hamma, and E. R. Mucciolo, *Physical Review Letters* **115**, 267206 (2015).